Gulf Journal of Mathematics
Vol 22, Issue 1 (2026) 1-22 ISSN: 2309-4966
https://doi.org/10.56947/gjom.v22i1.3945

FINE-TUNED CUBIC GENERALIZED COMPOSITE SPLINE INTERPOLATION WITH OPTIMAL PARAMETER

SEFTI RANIA[1*], SBIBIH DRISS[2] and JENNANE RACHID[3]

ABSTRACT. We develop a univariate C^2 generalized composite spline approximation method with an optimal parameter using Unified and Extended B-splines (UE-splines). These basis functions depend on a parameter that can be adjusted to minimize the error between data points and the approximation function. To determine the optimal parameter efficiently, we have introduced a fitting method based on genetic algorithms. This approach exploits the power of this algorithm. A numerical example is presented to analyze the effectiveness of our approach. We first examine the impact of the optimal parameter on the error bound and computational cost, and then compare our approximation model with existing interpolation methods.

Keywords. UE-splines, Generalized approximation, Composite Hermite interpolation, Genetic algorithm, optimal parameter.
2020 Mathematics Subject Classification. Primary 65D07; Secondary 68W50

1. INTRODUCTION

Splines are now widely used for modeling curves and surfaces to visualize and analyze available data in many domains, including engineering, computer graphics, and the science [4, 6, 12, 14, 5]. They are also crucial in the biomedical field, where splines play a significant role in anatomical modeling and medical image analysis [17, 18].Over the years, several types of splines for different spaces have been introduced in the literature, including NUAT splines [20], hyperbolic splines [9] and UE-splines [21]. The authors in [21] present a new algebraic space spanned by $\{\cos(\omega t), \sin(\omega t), 1, t, \dots, t^l, \dots\}$, which depends on a frequency parameter $\omega \in \mathbb{C}$. They provide a generalized definition of the spline basis functions associated with this space, called Unified and Extended splines (UE-splines). Several existing splines are special cases of UE-splines on different spaces. Moreover, most advantageous properties of classical polynomial B-splines are maintained.

Since the introduction of UE-splines, many researchers have adopted these generalized splines to solve various problems, making them a popular tool due to their advantageous modeling properties. Manni et al. presented in [10] an alternative

Date: Received: Dec 8, 2025; Revised: Jan 5, 2026; Accepted: Jan 15, 2026.
* Corresponding author

to the rational model based on generalized B-splines, providing the associated isogeometric analysis to overcome the limitations of the rational model in differentiation and integration. Bracco et al. extended in [1] the T-spline framework to generalized trigonometric T-splines by introducing a new family of functionals called TGT-splines, focusing on cases with constant frequency parameters. Lamnii et al. developed in [7] Marsden identities associated with the UE-spline space and introduced a generalized univariate quasi-interpolation spline based on these identities. Maqsood et al. introduced in [11] generalized trigonometric basis functions inspired by UE-splines, which preserve many geometric properties of classical Bernstein polynomials. They constructed the associated Bézier curve and demonstrated that the shape parameters provide a practical control for adjusting the shape of the curve by changing their values, rather than by changing the position of the control points.

Many existing methods in the literature have tested their models with given values of the adjustable parameter ω. Some studies have demonstrated, through numerous numerical tests, the existence of a frequency parameter that optimizes the approximation results. However, none of them have successfully found this optimal parameter. Finding this optimal parameter is a challenging task that can significantly improve the quality of the approximation in many practical problems. In this paper, we present a powerful algorithm for fitting the optimal parameter to the given dataset.

Genetic Algorithms (GA), introduced by Holland et al. in [3], are one of the most powerful techniques for solving complex optimization problems. Inspired by the laws of natural selection and genetics, they are among the evolutionary algorithms that have demonstrated impressive performance in solving complex optimization problems. The main idea of GAs is to replicate the process of natural evolution by iteratively improving a population of candidate solutions to a problem. These solutions are represented as chromosomes or genes and are manipulated using the genetic operations of selection, recombination or crossover, and mutation to simulate the processes of genetic recombination and mutation that occur in biological organisms. More broadly established in mathematics, genetic algorithms have received a lot of attention from researchers in various fields. GA find application in a wide range of optimization problems, including function optimization [2], parameter tuning [13], combinatorial optimization [22], and machine learning tasks [8].

In this paper, we present a novel cubic generalized composite spline approximation method based on uniform and extended spline basis functions. The obtained results can generalize various well-known Hermite interpolations in different spaces. Moreover, the composite partition associated with the obtained space of basis functions leads to a very small support, which improves the complexity of calculations. On the other hand, the basis functions depend on a parameter that can be adjusted for each data point. To determine the optimal parameter, we present a fitting method based on genetic algorithms. This technique has the advantage of a robust ability to iteratively explore the solution. This is done by encoding parameter solutions as chromosomes. Using this method, genetic algorithms can navigate through the search space to find the optimal solution to the problem. Moreover, in our approach, each chromosome contains only one gene representing the parameter, since we aim to find a single parameter that enhances the approximation accuracy. This simplified representation makes the GA-based fitting model less computationally expensive.

This paper proceeds as follows: Section 2 introduces a C^2 generalized composite spline Hermite interpolation function, analyzes its properties, and proves error estimates for the approximation. In Section 3, we present the parameter optimization algorithm, detail the chromosome coding of the optimization problem, and explain the various steps of the fitting process. Numerical experiments illustrating the performance of our approach are presented in Section 4, followed by a brief conclusion in Section 5.

2. Cubic generalized algebraic composite-spline interpolation

The goal of this section is to develop a unique generalized C^2 interpolation operator depending on a parameter ω that controls the quality of the interpolation. Before starting the construction of this operator, the following subsection presents some useful background information and initiations.

2.1. **Preliminaries and background.**

Let $k \geq 2$ and $\chi = x_i = a + 3ih_k{}_{i=0}^{n_k-1}$ represents a uniform partition of the interval $I = [a, b]$ into $n_k - 1$ sub-intervals, where $n_k = 2^k$ and $h_k = \frac{b-a}{3(n_k-1)}$. To create a cubic composite interpolant based on this partition, we first refine χ by adding two additional knots within each sub-interval $[x_i, x_{i+1}]$ for $i = 0, \ldots, n_k - 1$. More precisely, the refined partition is defined as follows:

$$\widetilde{\chi} = \{\widetilde{x}_i = a + \ ih_k,\ i = -3, \ldots, 3n_k\}, \tag{2.1}$$

where, for $i = 0, \ldots, n_k - 1$, $\widetilde{x}_{3i} = x_i$.

For a given frequency parameter $\omega = \sqrt{\alpha}$, where $\alpha \in \mathbb{R}$ and $\alpha \leq (\frac{\pi}{h_k})^2$, we define the spline space of order 4 with C^2 continuity over the partition $\widetilde{\chi}$ as:

$$S_4(I, \widetilde{\chi}) = \{S \in C^2(I) \ \setminus \ S_{|[\widetilde{x}_i, \widetilde{x}_{i+1}]} \in \mathbb{T}_4^\omega,\ i = 0, \ldots, 3n_k - 4\}, \tag{2.2}$$

where $\mathbb{T}_4^\omega$ is the space spanned by the set $\{cos(\omega x), sin(\omega x), 1, x\}$ for $x \in [x_i, x_{i+4})$.

The basis functions of the space $S_4(I, \widetilde{\chi})$ are the Unified and Extended B-spline (UE-spline) $N_{i,4}^\omega$ functions, as introduced in [21]. These functions are defined recursively as follows

$$N_{0,2}^\omega(x) = \begin{cases} \dfrac{\omega h_k sin(\omega x)}{2(1 - cos(\omega h_k))}, & 0 \leqslant x < h_k \\ \dfrac{\omega h_k sin(2\omega h_k - \omega x)}{2(1 - cos(\omega h_k))}, & h_k \leqslant x < 2h_k \\ 0, & \text{otherwise} \end{cases} \tag{2.3}$$

and for all i, $N_{i,2}^\omega(x) = N_{0,2}^\omega(x - x_i)$.
For $l \geqslant 3$, $N_{i,l}^\omega$ is defined by

$$N_{i,l}^\omega(x) = \frac{1}{h_k} \int_{x-h_k}^{x} N_{i,l-1}^\omega(s) ds \tag{2.4}$$

Remark 1.
- The support of the UE-spline $N^{\omega}_{i,4}$ is $[\widetilde{x}_i, \widetilde{x}_{i+4}]$.
- UE-splines have the same properties as usual B-splines (positivity, partition of unity, linear independence, etc.).
- Any spline function $S \in S_4(I, \widetilde{\chi})$ admits a unique representation in terms of the B-spline basis $\{N^{\omega}_{i,4}\}$:

$$S(x) = \sum_{i=-3}^{3n_k-4} a_i N^{\omega}_{i,4}(x). \tag{2.5}$$

Remark 2. The ω parameter can be a non-zero positive real number ($\alpha > 0$), zero ($\alpha = 0$), or a purely imaginary number ($\alpha < 0$). In addition, UE-spline basis functions coincide with other existing splines in special cases, such as

- Usual algebraic polynomial splines: for $\omega \equiv 0$ (ω in neighborhood of zero).
- Algebraic trigonometric splines: for $\omega = 1$.
- Algebraic hyperbolic splines: for $\omega = \imath$.

2.2. **Interpolation construction and properties.** For a given dataset $f^{(r)}(x_i),\ i = 0, \ldots, n_k - 1;\ r = 0, 1, 2,$ the C^2 generalized Hermite interpolation operator $\mathfrak{I}^{\omega}$, satisfies the following conditions:

$$\mathfrak{I}^{\omega} f^{(r)}(x_i) = f^{(r)}(x_i),\ i = 0, \ldots, n_k - 1;\ r = 0, 1, 2. \tag{2.6}$$

We define the generalized composite-spline Hermite basis of the space $S_4(I, \widetilde{\chi})$ by $\{\phi^{\omega}_{i,r},\ i = 0, \ldots, n_k - 1;\ r = 0, 1, 2\}$, satisfying:

$$\phi^{\omega^{(s)}}_{i,r}(x_j) = \delta_{i,j}\ \delta_{r,s},\ \text{for } i, j \in \{0, \ldots, n_k - 1\},\quad r, s \in \{0, 1, 2\}$$

where $\delta_{i,j}$ represents the Kronecker delta function.

Theorem 1. The Hermite interpolation problem with data $\{f^{(r)}(x_i),\ i = 0, \ldots, n_k - 1;\ r = 0, 1, 2\}$ has a unique solution $\mathfrak{I}^{\omega} f \in S_4(I, \widetilde{\chi})$ given by

$$\mathfrak{I}^{\omega} f(x) = \sum_{i=0}^{n_k-1} \sum_{r=0}^{2} f^{(r)}(x_i) \phi^{\omega}_{i,r}(x) \tag{2.7}$$

where

$$\phi^{\omega}_{i,0}(x) = N^{\omega}_{3i-3,4}(x) + N^{\omega}_{3i-2,4}(x) + N^{\omega}_{3i-1,4}(x),$$
$$\phi^{\omega}_{i,1}(x) = -h_k N^{\omega}_{3i-3,4}(x) + h_k N^{\omega}_{3i-1,4}(x),$$
$$\phi^{\omega}_{i,2}(x) = \frac{1 - \omega h_k cot(\omega h_k)}{\omega^2} N^{\omega}_{3i-3,4}(x) + \frac{1 - \omega h_k csc(\omega h_k)}{\omega^2} N^{\omega}_{3i-2,4}(x) + \frac{1 - \omega h_k cot(\omega h_k)}{\omega^2} N^{\omega}_{3i-1,4}(x).$$

Proof. Let $\phi^{\omega}_{i,r} \in S_4(I, \widetilde{\chi})$ for $i = 0, \ldots, n_k - 1$ and $r = 0, 1, 2$, each basis function can be represented as $\phi^{\omega}_{i,r}(x) = \sum_{j=-3}^{3n_k-4} a^r_{i,j}\ N^{\omega}_{j,4}(x)$ for suitable coefficients $\{a^r_{i,j}\}_{j=-3}^{3n_k-4}$. To obtain a Hermite approximant, the following conditions must be satisfied for all $l = 0, \ldots, n_k - 1,\quad \phi^{\omega^{(s)}}_{i,r}(x_l) = \delta_{i,l}\delta_{r,s}$. Moreover, since the support of $N^{\omega}_{j,4}$ is $[\widetilde{x}_j, \widetilde{x}_{j+4}]$, we get the following system of equations for all $l \in \{0, \dots, n_k - 1\}$:

$$\begin{cases} \dfrac{\omega h_k - sin(\omega h_k)}{2\omega h_k(1-cos(\omega h_k))} a^r_{i,3l-3} + \dfrac{sin(\omega h_k) - \omega h_k cos(\omega h_k)}{\omega h_k(1-cos(\omega h_k))} a^r_{i,3l-2} + \dfrac{\omega h_k - sin(\omega h_k)}{2\omega h_k(1-cos(\omega h_k))} a^r_{i,3l-1} & = \delta_{i,l}\delta_{r,0}, \\ -\dfrac{1}{2h_k} a^r_{i,3l-3} + \dfrac{1}{2h_k} a^r_{i,3l-1} & = \delta_{i,l}\delta_{r,1}, \\ \dfrac{\omega sin(\omega h_k)}{2h_k(1-cos(\omega h_k))} a^r_{i,3l-3} - \dfrac{\omega sin(\omega h_k)}{h_k(1-cos(\omega h_k))} a^r_{i,3l-2} + \dfrac{\omega sin(\omega h_k)}{2h_k(1-cos(\omega h_k))} a^r_{i,3l-1} & = \delta_{i,l}\delta_{r,2}. \end{cases} \tag{2.8}$$

The invertibility of the matrices associated with the system (2.8) ensures the existence of a unique solution, which is expressed as

$$\begin{pmatrix} a^0_{i,3i-3} \\ a^0_{i,3i-2} \\ a^0_{i,3i-1} \end{pmatrix} = \begin{pmatrix} 1 \\ 1 \\ 1 \end{pmatrix}, \begin{pmatrix} a^1_{i,3i-3} \\ a^1_{i,3i-2} \\ a^1_{i,3i-1} \end{pmatrix} = \begin{pmatrix} -h_k \\ 0 \\ h_k \end{pmatrix} \text{ and } \begin{pmatrix} a^2_{i,3i-3} \\ a^2_{i,3i-2} \\ a^2_{i,3i-1} \end{pmatrix} = \begin{pmatrix} \dfrac{1-\omega h_k cot(\omega h_k)}{\omega^2} \\ \dfrac{1-\omega h_k csc(\omega h_k)}{\omega^2} \\ \dfrac{1-\omega h_k cot(\omega h_k)}{\omega^2} \end{pmatrix}$$

Hence, we get the results.
Furthermore, the linear independence of the family $\{\phi^{\omega}_{i,r}\}$ can be derived directly. Indeed, since the set $\Phi^{\omega} = \{\phi^{\omega}_{i,r}\ ,\ i = 0, \dots, n_k - 1,\ r = 0, 1, 2\}$ contains exactly $\dim S_4(I, \widetilde{\chi})$ elements, it implies that Φ^{ω} is a basis for $S_4(I, \widetilde{\chi})$. $\square$

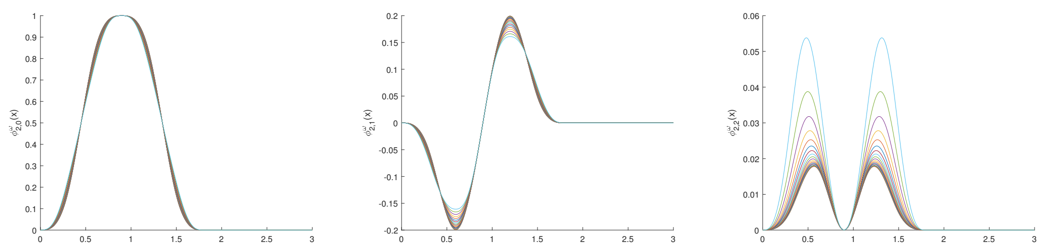

FIGURE 1. Effect of ω on basis functions $\phi^{\omega}_{2,0}$ (left), $\phi^{\omega}_{2,1}$ (middle), and $\phi^{\omega}_{2,2}$ (right) for $k = 3$, shown for several values of ω.

In Figure 1 we display the graphs of the basis functions $\phi^{\omega}_{2,0}$, $\phi^{\omega}_{2,1}$ and $\phi^{\omega}_{2,2}$ in the interval $[0, 2\pi]$ for various values of ω (positive real number and imaginary number) and for $k = 3$.

Example.

1. If $\omega \equiv 0$, the usual algebraic composite Hermite basis functions $\phi^0_{i,r}, r = 0, 1, 2$ are given as follows:

$$\phi^0_{i,0}(x) = N^0_{3i-3,4}(x) + N^0_{3i-2,4}(x) + N^0_{3i-1,4}(x),$$
$$\phi^0_{i,1}(x) = -h_k N^0_{3i-3,4}(x) + h_k N^0_{3i-1,4}(x),$$
$$\phi^0_{i,2}(x) = \frac{h_k^2}{3} N^0_{3i-3,4}(x) - \frac{h_k^2}{6} N^0_{3i-2,4}(x) + \frac{h_k^2}{3} N^0_{3i-1,4}(x),$$

where we get the results by calculating the limits of $\phi^{\omega}_{i,r}, r = 0, 1, 2$ when ω tends to zero.

2. If ω is nonzero, we can easily check the basis function by replacing the parameter ω with its value. For example, the UAT-spline (Uniform Algebraic Trigonometric spline) composite basis functions $\phi^{1}_{i,r}, r = 0, 1, 2$ are expressed by:

$$\phi^1_{i,0}(x) = N^1_{3j-3,4}(x) + N^1_{3j-2,4}(x) + N^1_{3j-1,4}(x)$$
$$\phi^1_{i,1}(x) = -h_l N^1_{3j-3,4}(x) + h_l N^1_{3j-1,4}(x)$$
$$\phi^1_{i,2}(x) = (1 - h_l cot(h_l))N^1_{3j-3,4}(x) + (1 - h_l csc(h_l))N^1_{3j-2,4}(x) + (1 - h_l cot(h_l))N^1_{3j-1,4}(x).$$

These two examples are identical to the basic functions introduced in [4].

Property 2. For each $i = 0, ..., n_k - 1$ and $r = 0, 1, 2$, the support of the function $\phi^{\omega}_{i,r}$ corresponds to the interval

$$[\widetilde{x}_{3i-3}, \widetilde{x}_{3i+3}] = [x_{i-1}, x_{i+1}].$$

This compact support is achieved through composite interpolation, which provides not only an optimal estimate of the approximation error but also simplifies the computational process.

Property 3. The basis functions $\phi^{\omega}_{i,r},\ i = 1, \ldots, n_k - 1$ and $r = 0, 1, 2$, are characterized by the following asymptotic bounds:

$$\|\phi^{\omega}_{i,0}\| \leqslant 1; \quad \frac{1}{h_k}\|\phi^{\omega}_{i,1}\| \leqslant \frac{2}{5}; \text{ and } \frac{1}{h_k^2}\|\phi^{\omega}_{i,2}\| \leqslant \frac{2}{13}. \tag{2.9}$$

Proof. The partition of unity property of the UE-spline basis functions clearly states that $\|\phi^{\omega}_{i,0}\| \leqslant 1$ for all $i = 0, \ldots, n_k - 1$.

On the other hand, we have

$$\begin{aligned}
\frac{1}{h_k^2}|\phi^{\omega}_{i,2}(x)| &= \left| \frac{1 - \omega h_k cot(\omega h_k)}{\omega^2 h_k^2} N^{\omega}_{3i-3,4}(x) + \frac{1 - \omega h_k \csc(\omega h_k)}{\omega^2 h_k^2} N^{\omega}_{3i-2,4}(x) \right. \\
&\quad \left. + \frac{1 - \omega h_k cot(\omega h_k)}{\omega^2 h_k^2} N^{\omega}_{3i-1,4}(x) \right| \\
&\le \left| \max\left(\frac{1 - \omega h_k cot(\omega h_k)}{\omega^2 h_k^2}, \frac{1 - \omega h_k \csc(\omega h_k)}{\omega^2 h_k^2} \right) \right| \left(N^{\omega}_{3i-3,4}(x) + N^{\omega}_{3i-2,4}(x) + N^{\omega}_{3i-1,4}(x) \right) \\
&\le \max\left(\left| \frac{1 - \omega h_k cot(\omega h_k)}{\omega^2 h_k^2} \right|, \left| \frac{1 - \omega h_k \csc(\omega h_k)}{\omega^2 h_k^2} \right| \right).
\end{aligned}$$

As $k \geq 2$, the sequence (h_k) is decreasing, we have $h_k \in]0, h_2] =]0, \frac{b-a}{9}]$. Furthermore, the functions

$$\eta(t) = \frac{1 - \omega t \cot(\omega t)}{\omega^2 t^2}, \text{ and } \theta(t) = \frac{\omega t \csc(\omega t) - 1}{\omega^2 t^2}$$

are such that $\eta(t) \geq 0$ and $\theta(t) \geq 0$ for all $t \in]0, h_2[$.
On this interval, both functions $\eta(t)$ and $\theta(t)$ are monotone increasing. In particular, computing the derivative of $\eta(t)$ gives

$$\eta'(t) = \frac{-2 + \omega t \cot(\omega t) + \omega^2 t^2 \csc(\omega t)^2}{\omega^2 t^3}. \tag{2.10}$$

The Taylor expansions of $\cot(\omega t)$ and $\csc(\omega t)$ around zero give $\cot(t) = \frac{1}{t} - \frac{t}{3} + O(t^3)$ and $\csc(t) = \frac{1}{t} + \frac{t}{6} + O(t^3)$. Then we get :

$$\eta'(t) \simeq \frac{t^4}{36} \geqslant 0 \tag{2.11}$$

Therefore, η and θ are maximized at $h_2 = \frac{b-a}{9}$. The interval $I = [a, b]$ can be $[0, 1]$,$[\frac{-\pi}{2}, \frac{\pi}{2}]$, or $[0, 2\pi]$, depending on the function to be approximated. We consider the largest interval and assume that $b - a = 2\pi$. Moreover, as $\omega \leq \frac{\pi}{h_k}$, we get

$$\max\left(\left|\frac{1 - \omega h_k \cot(\omega h_k)}{\omega^2 h_k^2}\right|, \left|\frac{1 - \omega h_k \csc(\omega h_k)}{\omega^2 h_k^2}\right|\right) \leq \frac{2}{5}$$

Thus, we get $\frac{1}{h_k^2}\|\phi_{i,2}\| \leq \frac{2}{5}$. Similarly, we can prove that $\frac{1}{h_k}\|\phi_{i,1}\| \leq \sqrt{\frac{2}{9}}\pi \leq \frac{2}{13}$. This concludes the proof.

□

Remark 3. There exist many approximation problems in various areas where the dataset can be periodic, i.e. $f^{(r)}(a) = f^{(r)}(b)$, for all $r = 0, 1, 2$. In this case, we can easily prove that we have

$$\phi^{\omega}_{0,r} = \phi^{\omega}_{n_k-1,r}, \ r = 0, 1, 2$$

knowing that we used periodic UE-splines where we can define it for any $x \in [a, b]$ as follows

$$N^{\omega}_{i,4}(x) = \begin{cases} N^{\omega}_{i,4}(x) & \text{if } \ i = -3, \ldots, 3n_k - 7 \\ N^{\omega}_{i,4}(x) + N^{\omega}_{i,4}(x + b) & \text{if } \ i = 3n_k - 6, \ldots, 3n_k - 4. \end{cases} \tag{2.12}$$

Then, due to the linearly independence of the basis function $\phi^{\omega}_{i,r}$, the approximation functions $\mathfrak{I}_k$ is defined as :

$$\mathfrak{I}^{\omega} f(x) = \sum_{i=1}^{n_k-1} \sum_{r=0}^{2} f^{(r)}(x_i)\phi^{\omega}_{i,r}(x). \tag{2.13}$$

Property 4. The approximation defined in (2.7) is exact on the space of algebraic polynomials T^{ω}_4, spanned by $\{cos(\omega x), sin(\omega x), 1, x\}$, i.e.

$$\mathfrak{I}^{\omega} p = p, \quad \forall \ p \ \in \ \mathbb{T}^{\omega}_4. \tag{2.14}$$

Proof. Following the approach based on Marsden's identity for the generalized algebraic space [7], each basis function of $\mathbb{T}^{\omega}_4 = \langle \cos(\omega x), \sin(\omega x), 1, x\rangle$, admits a representation in the UE-spline space. In particular, we obtain:

$$1 = \sum_{i=-3}^{3n_k-4} N^{\omega}_{j,4}(x); \qquad cos(\omega x) = \sum_{i=-3}^{3n_k-4} \frac{\omega h_k cos(\omega \widetilde{x}_{i+2})}{sin(\omega h_k)} N^{\omega}_{i,4}(x),$$

$$x = \sum_{i=-3}^{3n_k-4} \widetilde{x}_{i+2} N^{\omega}_{i,4}(x); \qquad sin(\omega x) = \sum_{i=-3}^{3n_k-4} \frac{\omega h_k sin(\omega \widetilde{x}_{i+2})}{sin(\omega h_k)} N^{\omega}_{j,4}(x).$$

Then, for $p(x) = 1$, we have

$$\begin{aligned}
\mathfrak{I}^{\omega} p(x) &= \sum_{i=0}^{n_k-1} \sum_{r=0}^{2} p^{(r)}(x_i)\phi^{\omega}_{i,r}(x) = \sum_{i=0}^{n_k-1} \phi^{\omega}_{i,0}(x) \\
&= \sum_{i=0}^{n_k-1} N^{\omega}_{3i-3,4}(x) + N^{\omega}_{3i-2,4}(x) + N^{\omega}_{3i-1,4}(x) \\
&= \sum_{i=-3}^{3n_k-4} N^{\omega}_{i,4}(x) = 1 = p(x).
\end{aligned}$$

For $p(x) = x$, we have

$$\begin{aligned}
\mathfrak{I}^{\omega} p(x) &= \sum_{i=1}^{n_k-1} x_i \phi^{\omega}_{i,0}(x) + \phi^{\omega}_{i,1}(x) \\
&= \sum_{i=1}^{n_k-1} (\widetilde{x}_{3i} - h_k) N^{\omega}_{3i-3,4}(x) + \widetilde{x}_{3i} N^{\omega}_{3i-2,4}(x) + (\widetilde{x}_{3i} + h_k) N^{\omega}_{3i-1,4}(x) \\
&= \sum_{i=1}^{n_k-1} \widetilde{x}_{i+2} N^{\omega}_{i,4}(x) = x.
\end{aligned}$$

For $p(x) = cos(\omega x)$, we have

$$
\begin{aligned}
\mathfrak{I}^\omega p(x) &= \sum_{i=1}^{n_k-1} cos(x_i)\phi^\omega_{i,0}(x) - \omega sin(x_i)\phi^\omega_{i,1}(x) - \omega^2 cos(x_i)\phi^\omega_{i,2}(x) \\
&= \sum_{i=1}^{n_k-1} (\omega h_k cot(\omega h_k) cos(\omega x_i) + \omega h_k sin(\omega x_i)) N^\omega_{3i-3,4}(x) + \omega h_k cosin(\omega h_k) cos(\omega x_i) N^\omega_{3i-2,4}(x) \\
&+ (\omega h_k cot(\omega h_k) cos(\omega x_i) - \omega h_k sin(\omega x_i)) N^\omega_{3i-1,4}(x) \\
&= \sum_{i=1}^{n_k-1} \frac{\omega h_k}{sin(\omega h_k)} (cos(\omega h_k) cos(\omega x_i) + sin(\omega h_k) sin(\omega x_i)) N^\omega_{3i-3,4}(x) \\
&+ \frac{\omega h_k}{sin(\omega h_k)} cos(\omega x_i) N^\omega_{3i-2,4}(x) + \frac{\omega h_k}{sin(\omega h_k)} (cos(\omega h_k) cos(\omega x_i) - sin(\omega h_k) sin(\omega x_i)) N^\omega_{3i-1,4}(x) \\
&= \sum_{i=1}^{n_k-1} \frac{\omega h_k cos(\omega(x_i + h_k))}{sin(\omega h_k)} N^\omega_{3i-3,4}(x) + \frac{\omega h_k cos(\omega x_i)}{sin(\omega h_k)} N^\omega_{3i-2,4}(x) \\
&+ \frac{\omega h_k cos(\omega(x_i - h_k))}{sin(\omega h_k)} N^\omega_{3i-1,4}(x) \\
&= \sum_{i=1}^{n_k-1} \frac{\omega h_k cos(\omega \widetilde{x}_{3i+1})}{sin(\omega h_k)} N^\omega_{3i-3,4}(x) + \frac{\omega h_k cos(\omega \widetilde{x}_{3i})}{sin(h_k)} N^\omega_{3i-2,4}(x) + \frac{\omega h_k cos(\omega \widetilde{x}_{3i-1})}{sin(\omega h_k)} N^\omega_{3i-1,4}(x) \\
&= \sum_{i=-3}^{3n_k-4} \frac{\omega h_k cos(\omega \widetilde{x}_{i+2})}{sin(\omega h_k)} N^\omega_{i,4}(x) \\
&= cos(\omega x) = p(x).
\end{aligned}
$$

Similarly, for $p(x) = sin(\omega x)$, we obtain

$$\mathfrak{I}^\omega p(x) = sin(\omega x) = p(x).$$

Then, we have for all

$$p \in \mathbb{T}^\omega_4, \ \mathfrak{I}^\omega p = p.$$

$\square$

2.3. **Interpolation error.** We now examine the interpolation error arising from the composite interpolant $\mathfrak{I}^\omega$. For this purpose, we recall several differential operators and the generalized Taylor formula presented by Schumaker in [16].

Denote by $\mathcal{L}^\omega_m$ the linear differential operators defined by $\mathcal{L}^\omega_m = \mathbf{D}^{m-2}(\mathbf{D}^2 + \omega^2 \mathbf{I})$, where $\mathbf{D}$ and $\mathbf{I}$ are the differential and identity operators respectively.
Note that the operator $\mathcal{L}^\omega_m$ is null on the space $\mathbb{T}^\omega_m = \langle cos(\omega x), sin(\omega x), 1, x, \ldots, x^{m-3} \rangle$, i.e.

$$\mathcal{L}^\omega_m f = 0 \text{ for all } f \in \mathbb{T}^\omega_m.$$

We also denote by $\mathcal{G}_m^\omega$ the Green's function, which corresponds to $\mathcal{L}_m^\omega$ and is expressed as

$$\mathcal{G}_m^\omega = \begin{cases} (-1)^{\frac{m+2}{2}} \dfrac{1}{\omega^{m-1}} \sin(\omega(x-y)_+) + (-1)^{\frac{m}{2}} \dfrac{1}{\omega^{m-1}} \displaystyle\sum_{j=0}^{\frac{m-4}{2}} (-1)^j \dfrac{(\omega(x-y)_+)^{2j+1}}{(2j+1)!}, & \text{for } m \text{ even}, \\ (-1)^{\frac{m-1}{2}} \dfrac{1}{\omega^{m-1}} \cos(\omega(x-y)_+) + (-1)^{\frac{m+1}{2}} \dfrac{1}{\omega^{m-1}} \displaystyle\sum_{j=0}^{\frac{m-3}{2}} (-1)^j \dfrac{(\omega(x-y)_+)^{2j+1}}{(2j)!}, & \text{for } m \text{ odd}. \end{cases} \tag{2.15}$$

where $(\cdot)_+$ is the truncated power.
To see more properties of this function, we refer the reader to the work cited in [7].

Now let us represent the space given by

$$L_p^m[a,b] = \{f : \mathbf{D}^{m-1} f \text{ is absolutely continuous on } [a,b] \text{ and } \mathbf{D}^{m-1} f \in L_p[a,b]\}.$$

Lemma 5. Let $m \geq 1$ and $f \in L_1^m(I)$, with $I = [a,b]$. The generalized Taylor formula [7] is given by:

$$f(x) = u_f(x) + \int_a^b \mathcal{G}_m^\omega(x,t) \mathcal{L}_m^\omega f(t) dt, \tag{2.16}$$

where u_f is the unique element in $\mathbb{T}_m^\omega$ such that

$$\mathbf{D}^{j-1} f(a) = \mathbf{D}^{j-1} u_f(a).$$

Theorem 6. Let $f \in L_1^4(I)$. Then the interpolation error between a function f and its generalized composite spline approximant $\mathfrak{I}^\omega f$ defined in (2.7) is given by:

$$\|\mathfrak{I}^\omega f - f\| \leq \frac{59}{260} \widetilde{h}^4 \|\mathcal{L}_4^\omega f\|_{L_1}, \tag{2.17}$$

where $\widetilde{h}_k = x_{i+1} - x_i$ and $\|\cdot\|$ denotes the sup norm in I.

Proof. Let $x \in I$, by using the Taylor's generalized formula (2.16) of order four, we get:

$$f(x) = u_f(x) + \int_a^b \mathcal{G}_4^\omega(x,t) \mathcal{L}_4^\omega f(t) dt, \tag{2.18}$$

this expression is equivalent to

$$f(x) = u_f(x) + \int_a^x \frac{-\sin(\omega(x-t)) + \omega(x-t)}{\omega^3} \mathcal{L}_4^\omega f(t) dt.$$

Recalling that the approximation function $\mathfrak{I}^\omega$ is exact on the space $\mathbb{T}_4^\omega$ and since $u_f \in \mathbb{T}_4^\omega$ therefore, $\mathfrak{I}^\omega u_f = u_f$.
Consequently, if we apply the operator $\mathfrak{I}^\omega$ to the function f, we obtain:

$$\mathfrak{I}^\omega f(x) = u_f(x) + \mathfrak{I}^\omega R_4(x),$$

where $R_4^\omega(x) = \displaystyle\int_a^x \frac{-\sin(\omega(x-t)) + \omega(x-t)}{\omega^3} \mathcal{L}_4^\omega f(t) dt.$

On the other hand, since $x \in I$, there exists $p \in \{0, \ldots, n_k - 2\}$ such that $x \in [x_p, x_{p+1}]$. Then, for $y \in [x_p, x_{p+1}]$ we have

$$f(x) = u_f(x) + \int_y^x \frac{-\sin(\omega(x-t)) + \omega(x-t)}{\omega^3} \mathcal{L}_4^\omega f(t) dt.$$

Therefore,

$$\mathfrak{I}^\omega f(y) - f(y) = \mathfrak{I}^\omega R_4^\omega(y) - R_4^\omega(y) = \mathfrak{I}^\omega R_4^\omega(y),$$

where

$$\mathfrak{I}^\omega R_4^\omega(y) = \sum_{i=1}^{n_k-1} \sum_{r=0}^{2} R_4^{\omega^{(r)}}(x_i) \phi_{i,r}^\omega(y).$$

Moreover, as $supp(\phi_{i,r}^\omega) = [\widetilde{x}_{3i-3}, \widetilde{x}_{3i+3}] = [x_{i-1}, x_{i+1}]$, $r = 0, 1, 2$, we deduce that only $\phi_{p,r}^\omega$ and $\phi_{p+1,r}^\omega$ intercept the interval $[x_p, x_{p+1}]$. Therefore,

$$\mathfrak{I}^\omega R_4^\omega(y) = \sum_{i=p}^{p+1} \sum_{r=0}^{2} R_4^{\omega^{(r)}}(x_i) \phi_{i,r}(y). \tag{2.19}$$

Indeed, for all $i \in \{\ p, p+1\ \}$ and for $k > 2$, using Taylor expansion of $sin(\cdot)$ in neighborhood of 0, we have $sin(\omega(x_i - t)) = \omega(x_i - t) - \frac{\omega^3(x_i-t)^3}{6} + O\left((\omega(x_i - t))^5\right)$. Then, we get

$$\begin{aligned}
|R_4^\omega(x_i)| &= \left| \int_y^{x_i} \frac{-\sin(\omega(x_i-t)) + \omega(x_i-t)}{\omega^3} \mathcal{L}_4^\omega f(t) dt \right| \\
&\leq \int_y^{x_i} \left| (\frac{(x_i-t)^3}{6}) \right| |\mathcal{L}_4^\omega f(t)|\, dt \\
&\leq \frac{1}{24} |x_i - y|^4 \|\ \mathcal{L}_4^\omega f\|_{L_1},
\end{aligned} \tag{2.20}$$

and

$$\begin{aligned}
|R_4^{\omega'}(x)| &\leq \|\mathcal{L}_4^\omega f\|_{L_1} \left| \frac{d}{dx} \left(\int_y^x \frac{-\sin(\omega(x-t)) + \omega(x-t)}{\omega^3} dt \right) \right| \\
&\leq \|\mathcal{L}_4^\omega f\|_{L_1} \left| \frac{-\sin(\omega(x-t)) + \omega(x-t)}{\omega^3} \right|.
\end{aligned}$$

Hence, we have

$$|R_4^{\omega'}(x_i)| \leq \frac{1}{6} |x_i - y|^3 \|\ \mathcal{L}_4^\omega f\|_{L_1}. \tag{2.21}$$

Similarly, using Taylor expansion of $\cos(\cdot)$ in neighborhood of 0, we have $cos(\omega(x_i - t)) = 1 - \frac{\omega^2(x_i-t)^2}{2} + O\left((\omega(x_i - t))^4\right)$,we have:

$$
\begin{aligned}
|R_4^{\omega^{(2)}}(x)| &\leq \|\mathcal{L}_4^\omega f\|_{L_1} \left| \frac{d^2}{dx^2} \left(\int_y^x \frac{-\sin(\omega(x-t)) + \omega(x-t)}{\omega^3} dt \right) \right| \\
&\leq \|\mathcal{L}_4^\omega f\|_{L_1} \left| \frac{-\omega\cos(\omega(x-y)) + \omega}{\omega^3} \right|.
\end{aligned}
$$

Therefore,

$$
|R_4^{\omega^{(2)}}(x_i)| \leq \frac{1}{2} |x_i - y|^2 \|\mathcal{L}_4^\omega f\|_{L_1}. \tag{2.22}
$$

On the other hand, according to (2.19), we have

$$
\begin{aligned}
|\mathfrak{I}_k R_4^\omega(y)| \leqslant{}& |R_4^\omega(x_p)\phi_{p,0}(y)| + |\ R_4^{\omega^{(1)}}(x_p)\phi_{p,1}(y)| + |R_4^{\omega^{(2)}}(x_p)\phi_{p,2}(y)| \\
&+ |R_4^\omega(x_{p+1})\phi_{p+1,0}(y)| + |R_4^{\omega^{(1)}}(x_{p+1})\phi_{p+1,1}(y)| \ + \ |\ R_4^{\omega^{(2)}}(x_{p+1})\phi_{p+1,2}(y)|.
\end{aligned}
$$

Using the inequalities in (2.9) alongside (2.20), (2.21), and (2.22), we obtain

$$
\begin{aligned}
\|\mathfrak{I}_k R_4^\omega\| \leq{}& |\ R_4(x_p)|\|\phi_{p,0}\| + |R_4^{\omega^{(1)}}(x_p)|\ \|\phi_{p,1}\| + |R_4^{\omega^{(2)}}(x_p)|\|\phi_{p,2}\| + |R_4^\omega(x_{p+1})|\ \|\phi_{p+1,0}\| \\
&+ |R_4^{\omega^{(1)}}(x_{p+1})|\|\phi_{p+1,1}\| + |\ R_4^{\omega^{(2)}}(x_{p+1})|\ \|\phi_{p+1,2}\| \\
&\leq (\|\phi_{p,0}\| + \|\phi_{p+1,0}\|) \frac{1}{24}(x_i - y)^4 \|\mathcal{L}_4^\omega f\|_{L_1} + (\|\phi_{p,1}\| + \|\phi_{p+1,1}\|) \frac{1}{6}(x_i - y)^3 \|\mathcal{L}_4^\omega f\|_{L_1} \\
&+ (\|\phi_{p,2}\| + \|\phi_{p+1,2}\|) \frac{1}{2}(x_i - y)^2 \|\mathcal{L}_4^\omega f\|_{L_1} \\
&\leq 2 \left(\frac{1}{24} \widetilde{h}^4 \|\mathcal{L}_4^\omega f\|_{L_1} + \frac{2}{5} \times \frac{1}{6} \widetilde{h}^4 \|\mathcal{L}_4^\omega f\|_{L_1} + \frac{2}{13} \frac{1}{2} \widetilde{h}^4 \|\mathcal{L}_4^\omega f\|_{L_1} \right) \\
&\leq \frac{59}{260} \widetilde{h}^4 \|\mathcal{L}_4^\omega f\|_{L_1},
\end{aligned}
$$

where $\widetilde{h} = x_{i+1} - x_i = \dfrac{b-a}{2^k - 1}$.
Consequently, we obtain the expected result:

$$
\|\mathfrak{I}_k f - f\| \leq \frac{59}{260} \widetilde{h}^4 \|\mathcal{L}_4^\omega f\|_{L_1}.
$$

□

3. Genetic algorithm approach to parameter optimization

In genetic algorithms, chromosomes, also known as "individuals," represent sets of genes that encode independent variables, with each chromosome serving as a solution to a specified problem.

The purpose of this section is to explore the use of a genetic algorithm to determine the optimal frequency parameter ω that improves approximation results. This is achieved by iteratively adjusting ω, starting with an initial population set of parameters and evolving them using various genetic operators until the most suitable parameter is identified. The genetic algorithm simulates biological evolution by applying selection, crossover, and mutation operations to the parameter population, gradually refining the search for the best ω. Therefore, for any given input dataset as described in (2.6), there exists an optimal parameter that leads to the best approximation function as defined in (2.7). This optimization process aims to increase the accuracy and reliability of the approximation model by fine-tuning ω to the characteristics of the input data.

Initial population. To initiate the GA implementation, we begin by encoding our problem into genetic representations. In our context, individuals correspond to the frequency parameter ω, serving as candidate solutions for the optimization problem. Let $N \in \mathbb{N}$, the initial population Ω^0 consists of N individuals and is randomly generated, ensuring that each individual is within a specified range. Specifically,

$$\Omega^0 = \{\omega_1^0, \omega_2^0, \ldots, \omega_N^0\},$$

where $\omega_j^0 = \sqrt{\alpha_j^0},\ j = 1, \ldots, N$ represent the initial individuals (chromosomes), such that for all $j \in \{1, \ldots, N\}$, $\alpha_j^0 \leq \left(\frac{pi}{h_k}\right)^2$.

Fitness function and selection. The fitness function plays a crucial role in the GA process, as it quantitatively evaluates the suitability or fitness of a candidate solution (chromosome) to solve the given optimization problem. In simple terms, the quality of each chromosome is determined by calculating the value of the fitness function. To find the optimal value of the parameter ω using the proposed interpolation operator $\mathfrak{I}^\omega$ defined in (2.7), we define the fitness function as the sup norm of the error between our interpolant and the dataset $f^{(r)}(x_i),\ i = 0, \ldots, n_k - 1;\ r = 0, 1, 2$ as follows:

$$\mathcal{F}(\omega) = \|\mathfrak{I}^\omega f - f\|, \tag{3.1}$$

Remark 4. When the function f is unknown and only discrete data $\{(x_j, y_j)\}_{j=0}^{M}$ are available, we select a subset of n_k knot points $\{(\tilde{x}_i, \tilde{y}_i)\}_{i=0}^{n_k-1}$ from the dataset. In this case, to construct the interpolant $\mathfrak{I}^\omega f$, we approximate the required derivatives using finite differences. For each knot $\tilde{x}_i$, where $(\tilde{x}_i, \tilde{y}_i) = (x_{p_i}, y_{p_i})$ where $p_i \in \{0, \ldots, M\}$, the first derivative is approximated by

$$f^{(1)}(\tilde{x}_i) \approx \frac{y_{p_i+1} - y_{p_i}}{x_{p_i+1} - x_{p_i}}, \quad i = 0, \ldots, n_k - 1,$$

The second derivatives are obtained as $f^{(2)}(\tilde{x}_i) = \mathcal{D} \circ \mathcal{D}(\tilde{x}_i)$. Then, the fitness function is calculated for all data points.

$$\mathcal{F}(\omega) = \underset{j=0,\ldots,M}{sup} |\mathfrak{I}^\omega f(x_j) - y_j|.$$

This approach enables the fitness function to control the quality of interpolation based on the value of each chromosome in the population $\Omega^t = \{\omega_1^t, \ldots, \omega_N^t\}$ at each generation t. Then the parents P^t are selected with an error threshold β_t

for reproduction within the population Ω^t by the following mechanism:

For all $t \in \tau$, where $\tau = \{0, 1, \ldots, t, ...\} \subset \mathbb{N}$ represents the set of generation numbers, and for all $j = 1, \ldots, N$, we have

$$\omega_j^t \in P^t, \text{ if and only if } \mathcal{F}(\omega_j^t) < \beta_t. \tag{3.2}$$

Genetic operators. After selecting parent individuals P^t, two essential genetic operators, crossover and mutation, are used to generate a new population Ω^{t+1} of solutions based on P^t. Crossover combines genetic material from two parent individuals to create two new recombinant offspring, thus promoting exploration by diversifying solutions. In contrast, mutation introduces randomness by changing individual genes, leading to new solutions and helping to avoid local optima. Together, these operators play a critical role in the GA's ability to adapt and evolve, ultimately improving its efficiency in finding optimal solutions over multiple generations.

(1) **Crossover:** At each generation t, we introduce a crossover operation within the selected parent P^t, where successive individuals ω_k^t and ω_{k+1}^t have the chance to combine through two linear combinations as follows:

$$\tilde{\omega}_k^t = p_k \omega_k^t + (1 - p_k)\omega_{k+1}^t,$$

and

$$\tilde{\omega}_{k+1}^t = (1 - p_k)\omega_k^t + p_k \omega_{k+1}^t,$$

where $\tilde{\omega}_k^t$ and $\tilde{\omega}_{k+1}^t$ represent the children individuals resulting from crossover, and p_k is a randomly selected probability parameter.

(2) **Mutation:** In the final step, each child individual undergoes a Gaussian mutation. In this type of mutation, a randomly generated value η_k^t from a Gaussian distribution with mean μ and standard deviation σ is added to the gene value. The mutation process can be expressed as follows:

$$\omega_k'^t = \tilde{\omega}_k^t + \eta_k^t.$$

We denote the set of mutated children as $\mathcal{C}^t = \{\omega_k'^t,\ k = 1, \ldots, r\}$.

Thus, a new generation is evolved from the parent P^t and the mutated children such that

$$\Omega^{t+1} = P^t \cup \mathcal{C}^t.$$

Afterwards, we repeat the process of computing the fitness function, selection, crossover, and mutation operations. This iterative process generates successive generations aimed at finding the optimal individual parameter (frequency parameter ω) until the stopping criteria is met.

Stop Process. The stopping criteria are crucial for ensuring the convergence of the proposed GA algorithm in finding the optimal value of the frequency parameter ω. When the fitness values of the population stop improving over successive generations, it indicates that convergence to the optimal solution has been achieved. At this point, the selected values of the individuals reach equilibrium despite the application of genetic operators. This state means that the proposed model has converged to the desired solution.

The complete algorithm for the proposed GA process for fitting the optimal parameter ω is detailed in Algorithm 1.

Algorithm 1: Optimization algorithm for determining the optimal parameter ω using genetic Algorithms.

---

input : Dataset $f^{(r)}(x_i),\ i = 0, \dots, n_k - 1;\ r = 0, 1, 2.$
The constants: number of individuals in initial population N, the fitness threshold β, the crossover chance $cross$, the mean μ, standard deviation σ, and the mutation chance mut.

output: Optimal frequency parameter ω^f.
Cubic generalized algebraic composite-spline interpolation $\mathfrak{I}^{\omega^f} f$.

$\Omega \leftarrow \Omega^0 = \{\omega_1^0, \dots, \omega_N^0\}$ // Population initialization
$t \leftarrow 1$
while $t < t^{max}$ **do**
  for $k \leftarrow 1$ *to* N **do**
    $\mathfrak{I}^{\omega_k^t} f(x) \leftarrow \sum_{i=0}^{n_k-1} \sum_{r=0}^{2} f^{(r)}(x_i)\phi_{i,r}^{\omega_k^t}(x)$
    $\mathcal{F}(\omega_k^t) \leftarrow \|\mathfrak{I}^{\omega_k^t} f - f\|$ // The fitness function
    if $\mathcal{F}(\omega_k^t) < \alpha^t$ **then**
      $P^t \leftarrow Select[\omega_k^t]$ // Parents selection
    end
  end
  for $k \leftarrow 1$ *to* $N - 1$ **do**
    if $rand() < cross$ **then**
      $\tilde{\omega}_k^t \leftarrow p_k\omega_k^t + (1 - p_k)\omega_{k+1}^t,$ //Crossover
      $\tilde{\omega}_{k+1}^t \leftarrow (1 - p_k)\omega_k^t + p_k\omega_{k+1}^t,$
    end
    if $rand() < mut$ **then**
      $\eta_k^t \leftarrow Gaussian(\mu, \sigma),$ // Mutation
      $\omega_k'^t = \tilde{\omega}_k^t + \eta_k^t$
    end
  end
  $\Omega^t \leftarrow \{\omega_1'^t, \dots, \omega_N'^t\} \cup P^t$ // New population
  if $\Omega^t == \Omega^{t-1}$ **then**
    Exit loop // Convergence criteria
  end
  $t \leftarrow t + 1$
end
return (Ω^f)

---

4. Numerical results

In this section, we perform experiments to demonstrate the effectiveness of our proposed generalized interpolation function $\mathfrak{I}^{\omega}$ as defined in (2.7). We analyze the effect of the obtained optimal parameter ω on three different functions, namely f_1, f_2, and f_3. Additionally, we evaluate the computational cost of the GA algorithm by measuring the time and iterations required to achieve convergence to the optimal parameters. Furthermore, we include a comparative analysis with an existing differential quasi-interpolant Q_k of [7] to demonstrate the robustness of our approach.

To implement the proposed approximation model with the optimal parameter using GA, we used MATLAB R2022b. The population of the GA algorithm was initialized with 100 individuals, where α ranged within the interval $[-1000, \left(\frac{\pi}{h_k}\right)^2]$. The threshold β_t is chosen depending on the value of the fitness function at each generation t. Further details on the constants used are provided in Table 1.

Table 1. Constants used in the implementation of the proposed approximation model.

a	b	N	$cross$	μ	σ	mut	t^{max}
$\frac{-pi}{2}$	$\frac{pi}{2}$	100	0.8	0	1	0.2	100

For the development of the proposed approximation method, we consider of the following three functions defined on the interval $I = [-\frac{\pi}{2}, \frac{\pi}{2}]$:

$$f_1(x) = \frac{2\sin(x)+1}{\sin(x)+2},\ \ f_2(x) = \frac{1}{24}\exp^{\frac{1}{1+x^2}} + x\cos(x), \quad \text{and} \quad f_3(x) = xe^{-x^2/2}.$$

We define the error between a function f and its corresponding approximation $\mathfrak{I}f$ as follows:

$$E(\mathfrak{I}f) = \|\mathfrak{I}f - f\|,$$

where $\|\cdot\|$ denotes the sup norm in I.

4.1. Effect of optimal parameters on interpolation performance.

As part of our initial experiments, we examine the error evolution of the first six selected parent parameters $\omega_l,\ l = 1, \ldots, 6$ over generations for the three functions f_1, f_2, and f_3 for $k = 3$ such that $n_k = 2^k$. The results are shown in the table 2.

From the table 2, we observe that the error bound between the introduced interpolation function $\mathfrak{I}^{\omega}$ and the data function improves with each generation of optimal individuals in Ω^t. Notably, at the 7th generation, this error converges to close values for all the selected parameters in the three function cases.
The optimal values of the frequency parameter ω_r^f for the functions f_r, where $r = 1, 2, 3$, varying with different values of k, are presented in Table 3. As shown

TABLE 2. The error estimation between the functions f_1, f_2 and f_3 and our approximation method (2.7), evaluated over different generations t with $k = 3$.

	Generation	$E(\mathfrak{I}^\omega f)$			
f_1	$t = 1$	8.4928×10^{-5}	4.1221×10^{-4}	$8.3985\times^{-3}$	1.0240×10^{-2}
	$t = 3$	8.4928×10^{-5}	1.2529×10^{-4}	1.4563×10^{-4}	1.5922×10^{-4}
	$t = 7$	8.0959×10^{-5}	8.0962×10^{-5}	8.0970×10^{-5}	8.0974×10^{-5}
f_2	$t = 1$	7.3671×10^{-5}	7.4948×10^{-4}	6.4775×10^{-3}	1.2981×10^{-2}
	$t = 3$	1.4122×10^{-5}	1.5542×10^{-5}	2.2644×10^{-5}	2.3958×10^{-5}
	$t = 7$	1.3913×10^{-5}	1.3965×10^{-5}	1.3972×10^{-5}	1.3983×10^{-5}
f_3	$t = 1$	4.5532×10^{-5}	9.5948×10^{-5}	2.3693×10^{-4}	1.1713×10^{-3}
	$t = 3$	3.2181×10^{-5}	4.4736×10^{-5}	4.8626×10^{-5}	5.3301×10^{-5}
	$t = 7$	2.1266×10^{-5}	2.1454×10^{-5}	2.1472×10^{-5}	2.1510×10^{-5}

in this table, the optimal frequency parameter varies depending on the type of data points and the number of interpolation points.

TABLE 3. Final and optimal ω_r^f values for f_r with $r = 1, 2, 3$, on different k.

k	ω_1^f	ω_2^f	ω_3^f
3	1.8189	$1.0919 + 0.0030\imath$	$1.0936 + 0.0015\imath$
4	$1.8803 + 0.0023\imath$	$1.5863 + 0.1376\imath$	1.2023
5	$1.9290 + 0.0256\imath$	$1.4057 + 0.4458\imath$	$1.1090 + 0.0073\imath$
7	$1.9290 + 0.0256\imath$	$1.6980 + 0.0916\imath$	$1.6737 + 0.0143\imath$
9	$10.6110 + 0.5281\imath$	$20.7893 + 0.0069\imath$	$9.5487 + 4.2136\imath$

The next experiment aims to demonstrate the optimality of the discovered parameter value in minimizing the error bound of the proposed cubic generalized composite interpolation function (2.7). To achieve this, we compare the interpolation errors over different values of the parameter ω, including the GA-based optimal parameter ω_r^f with $r = 1, 2, 3$. This comparison is performed for different values of k. Tables 4, 5, and 6 show the results for the three data functions $f_r,\ r = 1, 2, 3$, respectively.

To visually compare the error evolution between our interpolation method using different test values of the parameter ω and the optimal parameter ω_r^f for $r = 1, 2, 3$, we present the results in Figure 2.

4.2. **Computational cost.** The computational cost of such iterative method is crucial to prove its efficiency and practicality. In this subsection, we delve into the numerical results regarding the computational cost of our method. This includes

TABLE 4. Error estimation between f_1 and our approximation method for different values of the parameters ω and k.

	$E(\mathfrak{I}^{\omega} f_1)$					
k \ ω	$31\imath$	$6+9\imath$	$20+\imath$	$\frac{45}{3}+13\imath$	$5+\frac{9}{2}\imath$	ω_1^f
3	1.3060×10^{-2}	3.2660×10^{-3}	5.9844×10^{-2}	1.0236×10^{-2}	1.3379×10^{-3}	$\mathbf{8.0945\times10^{-5}}$
4	2.5456×10^{-3}	1.8648×10^{-4}	7.4150×10^{-4}	6.2792×10^{-4}	7.1574×10^{-5}	$\mathbf{4.8861\times10^{-6}}$
5	9.4748×10^{-5}	1.0751×10^{-5}	3.6936×10^{-5}	3.5590×10^{-5}	4.0623×10^{-6}	$\mathbf{2.8449\times10^{-7}}$
7	3.0768×10^{-7}	3.8455×10^{-8}	1.2671×10^{-7}	1.2617×10^{-7}	1.4463×10^{-8}	$\mathbf{1.0536\times10^{-9}}$

TABLE 5. Error estimation between f_2 and our approximation method for different values of the parameters ω and k.

	$E(\mathfrak{I}^{\omega} f_2)$					
k \ ω	$31\imath$	$6+9\imath$	$20+\imath$	$\frac{45}{3}+13\imath$	$5+\frac{9}{2}\imath$	ω_2^f
3	1.0717×10^{-2}	2.8110×10^{-3}	5.9119×10^{-2}	8.8291×10^{-3}	1.7094×10^{-3}	$\mathbf{1.9394\times10^{-5}}$
4	9.1515×10^{-4}	1.4859×10^{-4}	6.1431×10^{-4}	5.1022×10^{-4}	5.8129×10^{-5}	$\mathbf{1.6208\times10^{-6}}$
5	6.2955×10^{-5}	8.3359×10^{-6}	2.9489×10^{-5}	2.8129×10^{-5}	3.2092×10^{-6}	$\mathbf{1.0725\times10^{-7}}$
7	2.4215×10^{-7}	2.9750×10^{-8}	1.0117×10^{-7}	1.1259×10^{-7}	1.1403×10^{-8}	$\mathbf{3.7072\times10^{-10}}$

TABLE 6. Error estimation between f_3 and our approximation method for different values of the parameters ω and k.

	$E(\mathfrak{I}^{\omega} f_3)$					
k \ ω	$31\imath$	$6+9\imath$	$20+\imath$	$\frac{45}{3}+13\imath$	$5+\frac{9}{2}\imath$	ω_3^f
3	1.7613×10^{-2}	1.6182×10^{-3}	3.2758×10^{-2}	5.0664×10^{-3}	6.7379×10^{-4}	$\mathbf{1.9308\times10^{-5}}$
4	1.2116×10^{-3}	8.6891×10^{-5}	3.5403×10^{-4}	2.9581×10^{-4}	3.3662×10^{-5}	$\mathbf{1.7096\times10^{-6}}$
5	4.4132×10^{-5}	4.9453×10^{-6}	1.7275×10^{-5}	1.6546×10^{-5}	1.8851×10^{-6}	$\mathbf{1.1056\times10^{-7}}$
7	1.4366×10^{-7}	1.7705×10^{-8}	5.9414×10^{-8}	5.8769×10^{-8}	6.7201×10^{-9}	$\mathbf{3.7234\times10^{-10}}$

examining the time required for convergence and the number of generations required to reach optimal solutions. These findings provide valuable perspectives on the scalability and performance of our method in real-world applications.

TABLE 7. Number of generations and time required to achieve optimal approximation results for the three data functions over different values of k.

	f_1		f_2		f_3	
k	Generations	Time (s)	Generations	Time (s)	Generations	Time (s)
3	19	6.1512	5	3.9583	20	4.9023
4	11	10.3869	12	1.51204	12	8.2886
5	16	49.1705	20	40.0078	18	43.3225
7	17	203.2917	20	156.4783	19	171.3402

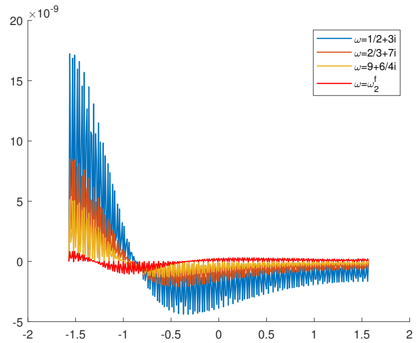

(A)

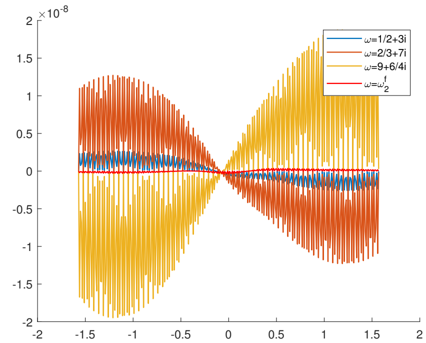

(B)

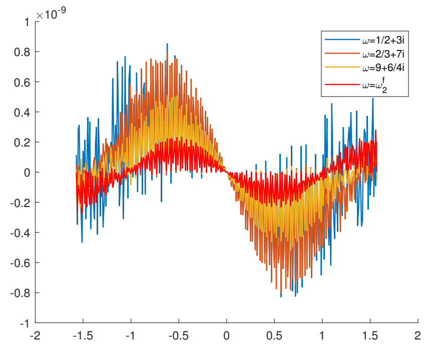

(C)

FIGURE 2. Comparison of the interpolation error evolution for the functions f_1 (a), f_2 (b), and f_3 (c) for $k = 7$ using different test ω values and optimal parameters ω_r^f $(r = 1, 2, 3)$.

As shown in Table 7, our proposed scheme achieves convergence within a few seconds using 8 GB of GPU memory, even with a large dataset size. This efficiency strongly supports the application of our model in real-world scenarios, especially when dealing with large datasets. It's worth noting that we used standard GPU memory; with more powerful hardware, the time required may be even more optimal.

4.3. **Comparison with similar approximation models.** To provide a comprehensive comparison of the performance of the proposed C^2 composite Hermite spline interpolant with optimal parameters against existing interpolation methods, we consider the following two test functions in the interval $[0, 1]$:

$$g_1(x) = -\frac{1}{1 + x + \log(1 + x^2)}, \ g_2(x) = e^{-x} \sin(5\pi x).$$

The optimal values of the parameter ω for the two examples of functions g_1 and g_2 are listed in Table 8:

TABLE 8. Optimal values of the parameter ω for the functions g_1 and g_2 for different values of k.

k	3	4	5	6	7
ω^{g_1}	3.8738	3.9559	$3.9758 + 0.04518\imath$	$4.0230 + 0.0905\imath$	$2.1500 + 6.2699\imath$
ω^{g_2}	15.7050	$15.7253 + 0.0159\imath$	15.7267	$15.7074 + 3.2901\imath$	$15.8250 + 0.3139\imath$

TABLE 9. Comparison by error estimations between the oscillatory quasi-interpolant [19] and the proposed interpolant.

k	$E(Qg_1)$ [19]	$E(\mathfrak{I}^\omega g_1)$	$E(Qg_2)$[19]	$E(\mathfrak{I}^\omega g_2)$
5	3.63×10^{-8}	$\mathbf{3.87 \times 10^{-9}}$	1.01×10^{-4}	$\mathbf{1.97 \times 10^{-6}}$
6	2.26×10^{-9}	$\mathbf{2.26 \times 10^{-10}}$	6.38×10^{-6}	$\mathbf{4.14 \times 10^{-7}}$
7	1.41×10^{-10}	$\mathbf{5.87 \times 10^{-11}}$	3.99×10^{-7}	$\mathbf{7.20 \times 10^{-9}}$

The obtained results from the error comparison in Table 9 clearly show a significant improvement in accuracy with our model compared to the existing oscillatory quasi-interpolant [19]. The computed errors show a marked reduction, indicating that our model outperforms the oscillatory quasi-interpolant significantly in terms of approximation accuracy.

5. CONCLUSION

In this paper, we introduced a new generalized composite Hermite spline basis function with optimal support and error bounds. Since the constructed interpolant depends on an adjustable parameter, we successfully identified the parameter that optimizes the interpolation results by drawing inspiration from genetic algorithms. The obtained numerical results demonstrate that our method efficiently achieves the optimal parameter, resulting in superior approximation accuracy compared to existing equivalent models. These promising results suggest that our method can be effectively applied in practical areas for modeling curves and surfaces in various domains.

REFERENCES

1. C. BRACCO, D. BERDINSKY, D. CHO, M. J. OH, T. W. KIM,Trigonometric generalized T-splines, (2014), Computer Methods in Applied Mechanics and Engineering, 268, 540-556. https://doi.org/10.1016/j.cma.2013.09.015
2. D. CHEN, Q. CHEN, A. S. LEON, R. LI, A genetic algorithm parallel strategy for optimizing the operation of reservoir with multiple eco-environmental objectives, (2016), Water resources management, 30, 2127-2142. https://doi.org/10.1007/s11269-016-1274-1
3. J. H. HOLLAND, Adaptation in natural and artificial systems: an introductory analysis with applications to biology, control, and artificial intelligence, , (1992), MIT press. https://doi.org/10.7551/mitpress/1090.001.0001
4. R. JENNANE, D. SBIBIH, AND R. SEFTI,(2024). C2 Composite Spline Methods for Fitting Data on the Sphere.,New Trends in Shape Modelling and Approximation Methods, 37, 61. https://doi.org/10.1007/978-3-031-62715-6_4

5. D. Joy, A. M. Regal, (2023). Tension spline approach to singularly perturbed delay differential equations involving large delay. Gulf Journal of Mathematics, 15(2), 166-174. https://doi.org/10.56947/gjom.v15i2.1314
6. A. Lamnii, H. Mraoui, D. Sbibih, A. Zidna, A multiresolution method for fitting scattered data on the sphere, (2009), BIT, 49(3), pp 589–610. https://doi.org/10.1007/s10543-009-0230-3
7. A. Lamnii, M. Y. Nour, D. Sbibih, A. Zidna,Generalized spline quasi-interpolants and applications to numerical analysis, (2022). Journal of Computational and Applied Mathematics, 114100. https://doi.org/10.1016/j.cam.2022.114100
8. L. Bi, G. Hu, A genetic algorithm-assisted deep learning approach for crop yield prediction, (2021),Soft Computing, 25, 10617-10628. https://doi.org/10.1007/s00500-021-05995-9
9. Y. Lü, G. Wang, X. Yang, Uniform hyperbolic polynomial B-spline curves, (2002), CAGD., 19(6), 379-393. https://doi.org/10.1016/S0167-8396(02)00092-4
10. C. Manni, F. Pelosi, M. L. Sampoli, Generalized B-splines as a tool in isogeometric analysis, (2011), Computer Methods in Applied Mechanics and Engineering, 200(5-8), 867-881. https://doi.org/10.1016/j.cma.2010.10.010
11. S. Maqsood, M. Abbas, G. Hu, A. L. A. Ramli, K. T. Miura, A novel generalization of trigonometric Bézier curve and surface with shape parameters and its applications, (2020), Mathematical Problems in Engineering, 2020, 1-25. https://doi.org/10.1155/2020/4036434
12. L. Qing, S. Shan, and W. Gao, Eigen-Harmonics Faces: Face Recognition under Generic Lighting, (2004). Proc. Sixth IEEE Intl Conf. Automatic Face and Gesture Recognition, pp.296–301. https://doi.org/10.1109/AFGR.2004.1301547
13. D. Saadaoui, M. Elyaqouti, K. Assalaou, S. Lidaighbi, Parameters optimization of solar PV cell/module using genetic algorithm based on non-uniform mutation, (2021), Energy Conversion and Management: X, 12, 100129. https://doi.org/10.1016/j.ecmx.2021.100129
14. S. Saidi, A Abbadi, M. Tahrichi,(2024). Estimating parametric surface areas using spline quasi-interpolants. Gulf Journal of Mathematics, 18(1), 54-71. https://doi.org/10.56947/gjom.v18i1.2370
15. I.J. Schoenberg, A. Sharma, Cardinal interpolation and spline functions v. the B-splines for cardinal hermite interpolation, (1973), Linear Algebra and its Applications, 7(1), 1-42. https://doi.org/10.1016/0024-3795(73)90034-7
16. L. L. Schumaker, Spline functions: basic theory, (2007), Cambridge University Press. https://doi.org/10.1017/CBO9780511618994
17. R. Sefti, D. Sbibih, and R. Jennane, (2025). An automatic B-snake model based on deep learning for medical image segmentation,Expert Systems with Applications, 270, 126481 https://doi.org/10.1016/j.eswa.2025.126481
18. R. Sefti, D. Sbibih, and R. Jennane,(2024). A CNN-based spline active surface method with an after-balancing step for 3D medical image segmentation,Mathematics and Computers in Simulation, 225, 607-618. https://doi.org/10.1016/j.matcom.2024.06.002
19. A. Serghini, A. Tijini, (2015). Construction of univariate spline quasi-interpolants with symmetric functions. Mathematics and Computers in Simulation, 118, 329-342. https://doi.org/10.1016/j.matcom.2014.11.028
20. G. Wang, Q. Chen, M. Zhou, NUAT B-spline curves, (2004), Comput. Aided Geom. Design, 21, pp. 193–205. https://doi.org/10.1016/j.cagd.2003.10.002
21. G. Wang, M. Fang, Unified and extended form of three types of splines, (2008), J. Comput. Appl. Math., 216, pp. 498–508. https://doi.org/10.1016/j.cam.2007.05.031
22. S. Zhou, L. Kang, G. Guo, Y. Zhang,, J. Cao, B. Cao, The application of combinatorial optimization by genetic algorithm and neural network, (2008, June), 3rd IEEE Conference on Industrial Electronics and Applications (pp. 227-231). IEEE. https://doi.org/10.1109/ICIEA.2008.4582512

[1] Higher School of Education and Training (ESEF), University Mohammed I, LANO Laboratory, Oujda Morocco.
Email address: sefti.rania@ump.ac.ma

[2] LANO Laboratory, University Mohammed I, FSO, Oujda Morocco.
Email address: sbibih@yahoo.fr

[3] IDP Laboratory, UMR CNRS 7013, University of Orleans, Orleans France.
Email address: rachid.jennane@univ-orleans.fr